

# Enhanced Thermoelectric Performance of Hybrid Nanoparticle–Single-Molecule Junctions

Elinor Zerah-Harush<sup>1</sup> and Yonatan Dubi<sup>1,2,\*</sup>

<sup>1</sup>*Department of Chemistry, Ben-Gurion University of Negev, Beer-Sheva 84105, Israel*

<sup>2</sup>*Ilse-Katz Institute for Nanoscale Science and Technology, Ben-Gurion University of the Negev, Beer-Sheva 84105, Israel*

(Received 19 February 2015; revised manuscript received 21 May 2015; published 23 June 2015)

It was recently suggested that molecular junctions would be excellent elements for efficient and high-power thermoelectric energy-conversion devices. However, experimental measurements of thermoelectric conversion in molecular junctions indicate rather poor efficiency, raising the question of whether it is indeed possible to design a setup for molecular junctions that will exhibit enhanced thermoelectric performance. Here we suggest that hybrid single-molecule–nanoparticle junctions can serve as efficient thermoelectric converters. The introduction of a semiconducting nanoparticle introduces new tuning capabilities, which are absent in conventional metal-molecule-metal junctions. Using a generic model for the molecule and nanoparticle with realistic parameters, we demonstrate that the thermopower can be of the order of hundreds of microvolts per degree kelvin and that the thermoelectric figure of merit can reach values close to 1, an improvement of 4 orders of magnitude over existing measurements. This favorable performance persists over a wide range of experimentally relevant parameters and is robust against disorder (in the form of surface-attached molecules) and against electron decoherence at the nanoparticle-molecule interface.

DOI: 10.1103/PhysRevApplied.3.064017

## I. INTRODUCTION

In recent years, the study of single-molecule junctions—the ultimate limit of electronic nanotechnology—has progressed well beyond their role as functional elements in electronic devices [1], and today, additional functionalities, from optoelectronics and spintronics through phononics to thermoelectricity [2–4], are under investigation. The potential applicability of single-molecule junctions in thermoelectricity—the conversion of heat into electric power—is of particular interest, since thermoelectricity may turn out to be an important element in addressing global energy issues [5,6]. The clear advantages of thermoelectric energy conversion, such as the “green” nature of the energy-conversion process, its applicability for waste-heat harvesting, and the easy device maintenance due to the absence of moving parts, lead us to think that thermoelectric devices should already be a substantial part of the energy market, yet this is not the case. The reason lies in the simple fact that current thermoelectric devices are not efficient enough, making competition with traditional (large-scale) energy-conversion systems virtually impossible.

Because of their versatility, low dimensionality, and low thermal conductivity, molecular junctions offer a possible route for enhancing thermoelectric performance [7]. Indeed, various theoretical studies suggest that molecular junctions can be a key component of efficient and high-power thermoelectric devices [8–16]. Experimental demonstrations

[17–26], however, indicate just the opposite, as can be deduced by examining the two central parameters of thermoelectric conversion, the thermopower (or the Seebeck coefficient) and the thermoelectric figure of merit (FOM).

The thermopower  $S$  measures the voltage generated per unit of temperature difference (in the linear response) [4,19,27,28]. The values of  $S \sim 10^2\text{--}10^3 \mu\text{V/K}$  are typical for standard semiconductor-based thermoelectrics, yet molecular junctions exhibit small values of  $S$ , typically  $S \sim 5\text{--}50 \mu\text{V/K}$ . The FOM, namely,  $ZT$ , defined as  $ZT = (GS^2)/(\kappa/T)$ , where  $G$  is the conductance of the junction,  $\kappa = \kappa_e + \kappa_{\text{ph}}$  is the total thermal conductance, which includes both electronic ( $e$ ) and phononic ( $\text{ph}$ ) contributions, and  $T$  is the temperature.  $ZT$  is directly related to the device efficiency [29], and  $ZT \rightarrow \infty$  corresponds to the Carnot efficiency (thus, theoretically, there is no upper bound on  $ZT$ ). It is commonly held that, from the efficiency perspective, a  $ZT$  of approximately 4 is required for thermoelectric conversion to be competitive [30]. However, typical  $ZT$  values obtained from measurements in molecular junctions are approximately  $10^{-3}\text{--}10^{-5}$ . Thus, there seems to be a discrepancy between theoretical and computational studies of thermoelectric conversion in molecular junctions, which in many cases [8–14] predict  $S \sim 10^2\text{--}10^3 \mu\text{V/K}$  and FOM of  $ZT \gg 1$ , and the experimental evaluation of the two measures.

The origin of this discrepancy seems to stem from two factors. First, one has to be careful to take the phonon contribution to the thermal conductance into account; a typical and realistic value for the phonon thermal conductance

\*jdubi@bgu.ac.il

in molecular junctions is  $\kappa_{\text{ph}} = 10\text{--}100 \mu\text{W/K}$  [13,19,31–33]. Second, many calculations show enhanced thermoelectric performance based on tuning of the molecular orbitals or, equivalently, the Fermi level of the electrodes. However, in reality, this tuning is very difficult to achieve [24,34–36], and the only “tuning parameter” available for molecular junctions is the choice of the molecular moiety. It is, thus, a central challenge to design molecular junctions that are both tunable in some way and show favorable thermoelectric performance with realistic parameters.

In this paper, we present a setup for molecular junctions that has the potential to achieve this goal. Our setup is based on a hybrid single-molecule–semiconducting-nanoparticle (SC-NP) structure in which a molecule is connected on one side to a metallic electrode (as in conventional molecular junctions), and on the other side, it is connected to the second electrode through a SC NP placed on the electrode, as is schematically depicted in Fig. 1(a). In this setup, the molecular junction can be tuned via tuning the electronic properties of the nanoparticle, namely, by choosing a suitable material and by controlling the size and shape of the nanoparticle (for reviews, see, e.g., Refs. [37–39]). The fabrication of hybrid NP–single-molecule junctions has already been demonstrated with Au NPs (see, e.g., Refs. [40–42]), making our suggested system experimentally feasible.

Using a generic model for the SC NP, we show that this junction can reach values of  $S \sim 100\text{--}400 \mu\text{V/K}$  and  $ZT$  of approximately 1 for a broad range of realistic parameters.

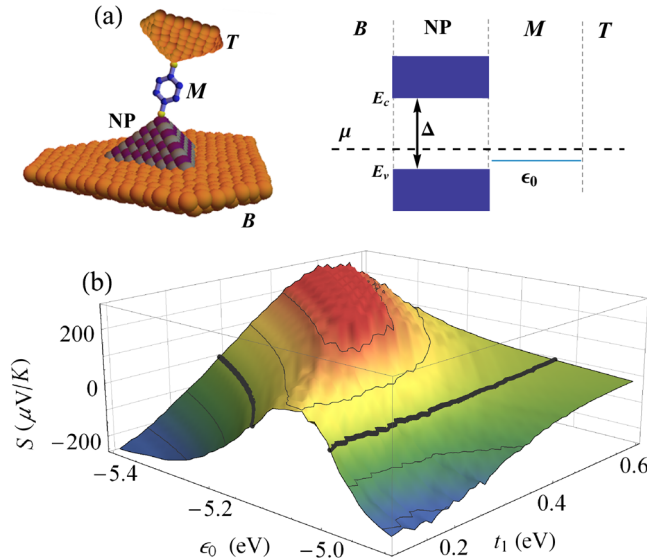


FIG. 1. (a) Schematic representation of the hybrid metal-molecule–nanoparticle–metal junctions (the choice of molecule is arbitrary) and the corresponding energy landscape. (b) Thermopower  $S$  as a function of the position of the molecular orbital  $\epsilon_0$  and molecule-nanoparticle coupling  $t_1$  for a hybrid molecular junction with a square-pyramid shape (see text for numerical parameters).

The origin of the enhanced thermoelectric performance can be traced to the interplay between the local transport properties of the molecule and the gapped density of states of the nanoparticle [13]. Thermoelectricity typically requires a large particle-hole asymmetry (reflected in the fact that, at low temperatures, the thermopower is proportional to the derivative of the transmission function [4,19,28]). This asymmetry is enhanced in this junction due to the presence of the semiconducting gap in the SC NP [13], an effect that is rectified due to the finite size of the nanoparticle. We show that the optimal parameters for thermoelectric conversion depend on the geometry of the nanoparticle and the contact geometry between the nanoparticle and the molecule. Further, we demonstrate that the favorable thermoelectric performance is robust against disorder (in the form of surface dangling molecules) and dephasing, and finally, we discuss the temperature dependence of the FOM, which exhibits a maximum at  $T \sim 450$  K.

## II. MODEL AND CALCULATION

The transport and thermoelectric properties of the hybrid molecule-nanoparticle junction are calculated by using the nonequilibrium Green’s function approach, which has become the standard tool for such calculations [27,28]. The junction [graphically depicted in Fig. 1(a)] is described using the Hamiltonian

$$\mathcal{H} = \mathcal{H}_B + \mathcal{H}_{\text{NP}} + \mathcal{H}_M + \mathcal{H}_T + \mathcal{H}_{B\text{-NP}} + \mathcal{H}_{\text{NP}\text{-}M} + \mathcal{H}_{M\text{-}T} \quad (1)$$

that includes the bottom electrode ( $B$ ), the nanoparticle ( $\text{NP}$ ), the molecule ( $M$ ), the top electrode ( $T$ ), and the coupling between the bottom electrode and nanoparticle ( $B\text{-NP}$ ), between the NP and the molecule ( $\text{NP}\text{-}M$ ), and between the molecule and the top electrode ( $M\text{-}T$ ). Since electron spin does not play a role in the mechanisms we describe here for enhancement of thermoelectricity, we treat spinless electrons.

To describe the SC NP, we use a generic tight-binding model for a semiconductor [43–48] of the form

$$\mathcal{H}_{\text{NP}} = \sum_{\mathbf{r}} \left[ \epsilon_c + \frac{\Delta}{2} (-1)^{P_{\mathbf{r}}} \right] c_{\mathbf{r}}^{\dagger} c_{\mathbf{r}} - t \sum_{\langle \mathbf{r}\mathbf{r}' \rangle} c_{\mathbf{r}}^{\dagger} c_{\mathbf{r}'}, \quad (2)$$

where the summation is taken over the atom positions  $\mathbf{r}$  (assumed to form a cubic lattice),  $c_{\mathbf{r}}^{\dagger} (c_{\mathbf{r}})$  creates (annihilates) an electron at position  $\mathbf{r}$ ,  $t$  is the nearest-neighbor hopping matrix element,  $\epsilon_c$  is the position of the band-gap center, and  $\Delta$  is the semiconductor band gap. The function  $P_{\mathbf{r}} = x + y + z$  gives a modulation of the on-site energy  $\epsilon_c \pm (\Delta/2)$  between neighboring atoms, generating a gapped band at the thermodynamic limit [44]. We point out that although *ab initio* methods for calculating properties of NPs are emerging [49,50], these are still not

developed for transport calculations. Furthermore, since we are aiming at presenting general properties of hybrid junctions, our tight-binding calculation is generic and not limited to a specific system.

The molecule is described as a single orbital, which can correspond to either the HOMO or LUMO, depending on the position of the orbital energy [28]. The molecular Hamiltonian is simply

$$\mathcal{H}_M = \epsilon_0 d^\dagger d, \quad (3)$$

where  $d^\dagger(d)$  creates (annihilates) an electron at the molecular orbital. In addition to the calculations described below, we perform calculations that also include a Coulomb interaction term (for the molecule) and spin-full fermions (by using the equations-of-motion method [51,52]) but find no quantitative change in the main results, and, therefore, we keep the description here as simple as possible and treat electrons as noninteracting particles. The coupling between the molecule and the nanoparticle is described by the Hamiltonian

$$\mathcal{H}_{\text{NP-M}} = -t_1 c_{\mathbf{r}_M}^\dagger d + \text{H.c.}, \quad (4)$$

where  $\mathbf{r}_M$  is the position of the atom in the nanoparticle that is in contact with the molecule, and  $t_1$  is the hopping matrix element related to the overlap integral between the molecular orbital and the atomic level at  $\mathbf{r}_M$ .

The metallic top and bottom electrodes are assumed to be noninteracting metals [53] with the Hamiltonian  $\mathcal{H}_X = \sum_k \epsilon_k c_{k,X}^\dagger c_{k,X}$ ,  $X = T, B$  [27,28,53]. The coupling between the molecule and the top electrode (representing, e.g., the tip of a scanning tunneling microscope) is represented by the Hamiltonian term  $\mathcal{H}_{M-T} = \sum_{k,T} V_{k,T} c_{k,T}^\dagger d + \text{H.c.}$  Similarly, the contact between the bottom electrode and the nanoparticle is described by  $\mathcal{H}_{B-MP} = \sum_{\mathbf{r} \in B} V_{k,B} c_{k,B}^\dagger c_{\mathbf{r}} + \text{H.c.}$  To proceed with the transport calculations, the metallic electrodes are treated within a wide-band approximation [54] (valid since our model is for noninteracting electrodes), where the top electrode is defined by a (retarded and advanced) self-energy term  $\Sigma_T^{r,a} = \mp i(\Gamma_T/2)|M\rangle\langle M|$ , in which  $|M\rangle$  is the single-particle molecular orbital, and  $\Gamma_T$  is the electrode-induced level broadening. Similarly, the bottom electrode is defined via the self-energy term  $\Sigma_B^{r,a} = \mp i(\Gamma_B/2)\sum_{\mathbf{r} \in B} |\mathbf{r}\rangle\langle \mathbf{r}|$ , where  $\Gamma_B$  is the broadening due to the bottom electrode, and the summation is taken over all the atom positions in the nanoparticle that are in contact with the bottom electrode. We point out that the model described above (and, specifically, the wide band approximation) implies electron-phonon-induced thermalization in the electrodes but no electron-phonon interaction in the junction at this stage. All the relevant energies—the Fermi level of the electrodes, NP valence and conduction bands, and molecular orbitals—are schematically shown in Fig. 1(a) also.

Once the Hamiltonian and the self-energies are defined, the calculation proceeds via the nonequilibrium Green's function approach, which is reduced to the Landauer formalism for noninteracting electrons [27,55,56]. The Green's functions are determined via  $G^{r,a} = (E - \mathcal{H} + \Sigma^{r,a})^{-1}$ , where  $\Sigma^{r,a} = \Sigma_T^{r,a} + \Sigma_B^{r,a}$ . The transmission function is given by  $T(E) = \text{Tr}(\Sigma_T^r G^r \Sigma_B^a G^a)$ , and the transport coefficients, namely, the conductance  $G$ , the thermopower  $S$ , and the thermal conductance  $\kappa$ , are determined within the Landauer formalism as  $G = e^2 L_0$ ,  $S = L_1/(eTL_0)$ ,  $\kappa = [L_2 - (L_1^2/L_0)]/T$ , where  $T$  is the temperature (room temperature, unless otherwise stated), and  $L_n = -(1/h) \int dE T(E) (E - \mu)^n (\partial f / \partial E)$  are the Landauer integrals, with  $h$  being Planck's constant,  $\mu$  the chemical potential of the electrodes, and  $f(E)$  the Fermi-Dirac distributions. The thermoelectric FOM  $ZT$  is given by  $ZT = (GS^2)/(\kappa/T)$ .

### III. RESULTS

We start by describing the thermopower  $S$  and FOM  $ZT$  for a single molecule placed on a square pyramid-shaped nanoparticle [57,58] (the bottom electrode is in contact with the [111] plane), as shown in Fig. 1(a). Since we present here a generic model for nanoparticles, we are not aiming to obtain quantitative results describing a specific system. We are, nonetheless, aware that it is essential to take numerical parameters that are realistic and readily describe experimental systems. We, thus, choose the semiconducting band center at  $\epsilon_c = -4.8$  eV and  $\Delta = 0.8$  eV, corresponding to PbSe nanoparticles and  $\mu = -5.1$  eV as the electrode chemical potential (corresponding to Au electrodes). Other numerical parameters are  $t = 1.6$  eV,  $\Gamma_B = 0.05$  eV, and  $\Gamma_T = 0.01$  eV (describing weakly coupled molecules, see, e.g., Ref. [59]). The pyramid basis contains  $10 \times 10$  atoms, and our results weakly (and quantitatively) depend only on the size of the nanoparticle.

In Fig. 1(b), we show the thermopower  $S$  as a function of molecular orbital energy level  $\epsilon_0$  and the molecule-nanoparticle coupling  $t_1$ . In experiments,  $\epsilon_0$  can be tuned by choice of molecule and by choice of the nanoparticle composition and size. The coupling  $t_1$  can be additionally tuned by stretching or squeezing the molecular junction with the top electrode [60–62]. As may be seen,  $S$  can reach values as high as  $\pm 200$   $\mu\text{V/K}$  and can change sign according to the position of the molecular level with respect to the semiconducting band edge.

The appearance of a thermopower maximum upon a change in  $\epsilon_0$  is not surprising, since one will expect that tuning  $\epsilon_0$  will lead to a near resonance in transmission (which implies a maximum thermopower). However, the appearance of a maximum upon a change of  $t_1$  is surprising; in a typical single-molecule junction, stretching the junction will lead only to a change in the molecule-electrode coupling and will not result in a thermopower

maximum. Here, since the molecule and the NP hybridize, changing  $t_1$  (experimentally—by means of pulling the junction) is similar to changing the molecular orbital, i.e., pulling the junction plays the role of gating. Since gating a molecular junction is a challenging task [24,34–36], this result puts an additional advantage on hybrid junctions.

To calculate  $ZT$ , we add to the electronic thermal conductance a phononic term  $\kappa_{\text{ph}} = 50$  pW/K, a realistic value for molecular junctions [19,31–33]. In Fig. 2, we plot the central result of this paper,  $ZT$  of the hybrid single-molecule–NP junction, as a function of  $\epsilon_0$  and  $t_1$ . The FOM reaches  $ZT > 0.8$ , i.e., more than 3 orders of magnitude larger than the values measured in regular molecular junctions. The realistic parameters considered here and the wide range of parameters in which  $ZT$  is large implies that this regime should be accessible for experiments.

In the inset of Fig. 2, we show  $ZT$  as a function of  $\epsilon_0$  for a constant  $t_1 = 0.1$  eV for three different configurations. The first (solid blue line) is the same as the setup in the main figure. In the second setup (dotted orange line), the molecule is in contact with a pyramid nanoparticle, but the positions of the  $\pm\Delta$  terms in the nanoparticle Hamiltonian of Eq. (2) are switched, modeling a change in the atom species at the apex of the nanoparticle (for instance, either Pb or Se in PbSe nanoparticles). The third setup (dashed green line) describes a molecule in contact with a cube-shaped (as opposed to a pyramid) nanoparticle. As may be seen, the contact configuration and the shape of the nanoparticle can have a strong effect on  $ZT$ ; although

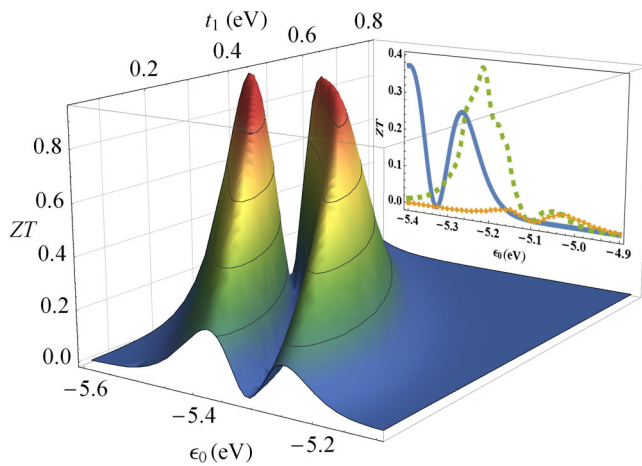


FIG. 2.  $ZT$  as a function of the position of the molecular orbital  $\epsilon_0$  and the molecule-nanoparticle coupling  $t_1$  for a hybrid molecular junction with a square-pyramid shape (see text for numerical parameters). Inset:  $ZT$  as a function of  $\epsilon_0$  for a constant  $t_1 = 0.1$  eV, for the hybrid junction with a pyramid nanoparticle (blue solid line), a pyramid nanoparticle with switched  $\pm\Delta$  positions (dotted orange line; see text), and a cube-shaped nanoparticle (dashed green line).

values of  $ZT > 0.8$  can be achieved in these configurations, the optimal parameters vary between the different setups.

In experiments, a reasonable situation is for additional molecules to attach to the surface of the nanoparticle. To model this scenario, we add to the Hamiltonian additional molecules, with the same orbital level  $\epsilon_0$  and coupling  $t_1$  but with a random coupling point to the surface of the nanoparticle (top inset in Fig. 3). The transport properties are then averaged over  $10^4$  realizations of random positions. In Fig. 3,  $ZT$  is plotted as a function of surface coverage (in percent) of attached molecules. Surprisingly, we find a slight increase of  $ZT$  for a small number (approximately 8%) of attached molecules, followed by a decrease in  $ZT$  when the number of attached molecules is increased. To elucidate the origin of this result, the lower inset shows the average conductance (blue circles) and thermopower (orange triangles) as a function of surface coverage (in percent). We find that the average conductance actually increases with the number of surface molecules, but the thermopower decreases, thus, eventually leading to a decrease in  $ZT$ .

The origin of this effect is the fact that the surface coverage induces two competing processes. On one hand, the addition of molecules bound to the surface adds conduction channels (i.e., local resonances in the transmission function) and, therefore, increases the conductance. On the other hand, the presence of disorder tends to flatten the resonances on average. As a result, the thermopower, which is proportional to the derivative of the transmission function [4], becomes smaller as the transmission resonance becomes wider. This competition is reflected in the opposite trends of  $G$  and  $S$  in the inset of Fig. 3. Since  $ZT$  is the product of the conductance which increases and the thermopower which decreases, it exhibits nonmonotonic behavior.

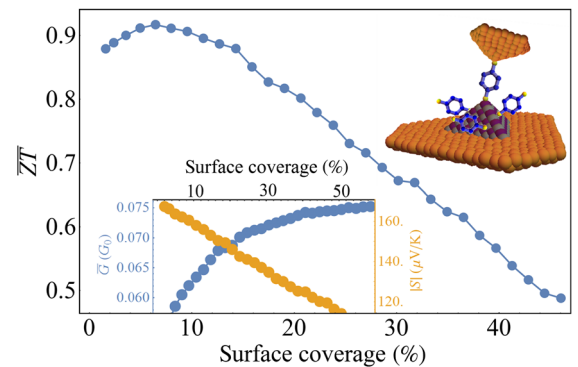


FIG. 3.  $ZT$  as a function of surface coverage (in percent) of molecules attached to the nanoparticle surface. Upper inset: Schematic representation of the surface-attached molecules. Lower inset: Average conductance (blue circles) and thermopower (orange triangles) as a function of the number of surface molecules.

At room temperature, it is possible that the electron motion across the junction will not be coherent and that the electrons will dephase as they cross the molecule-NP interface. This may occur due to the interaction of electrons with the (soft) phonons of the NP or due to vibrations in the position of the molecule with respect to the electrodes (but not due to interaction of electrons with the molecular vibrations, which are typically high-energy modes; such interactions were discussed in, e.g., Ref. [63]). If such dephasing is present, the formulation presented above is invalid, as it describes coherent transport. To account for decoherence, we note that if the electron loses its phase on the molecule-NP interface, then the NP can, in fact, be considered as a semiconducting electrode. This results in an effective SC-molecule-metal junction, which can again be described using the Landauer formula, with the appropriate choice of self-energies.

To model the SC electrode, we recall that the imaginary part of the self-energy describes the electrode density of states. Similar to the wide-band approximation for the metallic electrode, we model the semiconducting electrode as constant outside the gap and zero in the gap. The imaginary part of the semiconducting self-energy can, thus, be written with the use of a Heaviside step function  $\Theta$  as  $\text{Im}\Sigma_{\text{SC}} = \Gamma_B/2\{\Theta[|E - \epsilon_c| - (\Delta/2)]\}$  and the real part of the self-energy determined via the Kramers-Kronig relation [27,64]. In the numerical calculations given below, the step-function discontinuity is broadened by 0.01 eV, a value that can arise in realistic systems from lattice impurities and dislocations or thermal fluctuations.

In Fig. 4, we plot the 4(a) conductance, 4(b) thermopower, 4(c) thermal conductance, and 4(d)  $ZT$  for the hybrid SC-NP-molecule-metal junction (solid lines) as a function of  $\epsilon_0$ , with  $\Gamma_B = 0.05$  eV,  $\Gamma_T = 0.01$  eV,  $\epsilon_c = -4.8$  eV, and  $\Delta = 0.8$  eV. Looking at  $ZT$ , we find

that the dephasing process in the NP does not substantially reduce the maximal  $ZT$  from the coherent case (the maximal value of Fig. 2). For comparison, the dashed lines of Figs. 4(a)–(d) show the same for  $\Delta = 0$ , i.e., a “standard” metal-molecule-metal ( $M-M-M$ ) junction. The two most striking features of the comparison between the hybrid junction and the  $M-M-M$  junction are (i) the thermopower is substantially larger for the hybrid junction and over a wider range of  $\epsilon_0$ , and (ii)  $ZT$  of the hybrid junction is roughly twice as large as that of the  $M-M-M$  junction.

The inset of Fig. 4(d) shows the inverse Lorenz number  $L_0/L$  as a function of  $\epsilon_0$  for the hybrid junction (solid line) and  $M-M-M$  junction (dashed line). While a violation of the Wiedeman-Franz (WF) law  $L_0/L \sim 1$  is observed for both types of junctions, the hybrid junction shows a much larger violation, which, in fact, determines the position of the maximal  $ZT$ , while for the  $M-M-M$  junction, the position of the maximal  $ZT$  is determined by the maximum of  $S$ .

Up till now, we considered a molecule which is weakly coupled to the electrodes. However, depending on the chemical moiety, the coupling between the molecule and the electrodes can be much larger (see, e.g., Refs. [9,10,59]). It is, therefore, of interest to see whether the increase in  $ZT$  in hybrid junctions compared to the  $M-M-M$  junctions is maintained also for strongly coupled molecules. In Figs. 4(e)–4(h), the same as in Figs. 4(a)–4(d) is plotted for a strongly coupled molecule, with  $\Gamma_B = 0.5$  eV,  $\Gamma_T = 0.1$  eV. Again, the two most striking differences between the hybrid junction and the  $M-M-M$  junction are the thermopower and  $ZT$ , which are even more profound for the strongly coupled junction. Because of the large value of the coupling, the transmission resonance of the  $M-M-M$  junction is very broad, and, therefore, the

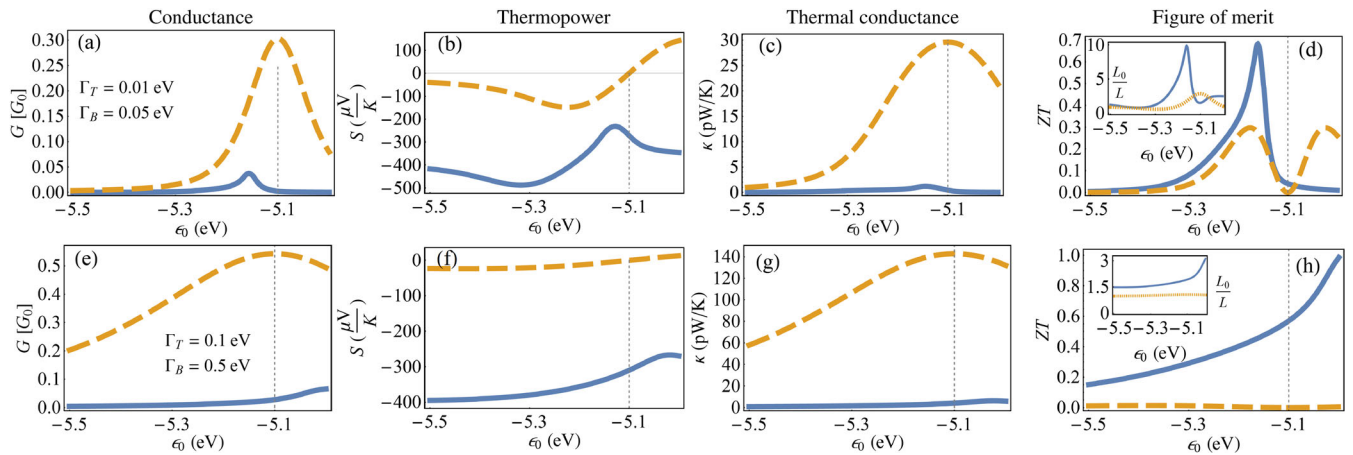


FIG. 4. (a) Conductance, (b) thermopower, (c) thermal conductance, and (d)  $ZT$  as a function of molecular orbital energy  $\epsilon_0$ , for a semiconductor-molecule-metal junction (solid lines) and a metal-molecule-metal junction (dashed lines) calculated for a weakly coupled molecule ( $\Gamma_B = 0.05$  eV,  $\Gamma_T = 0.01$  eV). Inset of (d): Inverse Lorenz number as a function of  $\epsilon_0$ . (e)–(h) Same as (a)–(d), for a strongly coupled molecule ( $\Gamma_B = 0.5$  eV,  $\Gamma_T = 0.1$  eV).

thermopower is very small. That, in addition with the fact that the WF law is obeyed [shown in the inset of Fig. 4(h), dashed line] results in a small  $ZT$  of approximately  $10^{-2}$ . In contrast, the hybrid junction (solid lines) shows only a slight reduction of the thermopower [Fig. 4(f)], because although the molecular level is broadened due to the metallic lead, the band edge of the SC electrode still introduces a sharp feature to the transmission function. Along with a violation of the WF law [inset of Fig. 4(h)], this leads to a relatively large  $ZT$  of approximately 1. Surprisingly,  $ZT$  for the strongly coupled hybrid junction displays larger  $ZT$  than the weakly coupled junction, with large values of  $ZT$  for  $\epsilon_0$  well inside the SC band gap (as a result of the WF law violation inside the gap).

As was noted earlier, one of the advantages of the hybrid NP-molecule junctions is the ability to tune not the molecular orbitals but the SC-NP band structure with this ability in mind, in Fig. 5 we plot  $ZT$  for a constant value of the molecular orbital  $\epsilon_0 = -5.2$  eV, as a function of the band gap  $\Delta$  [the band center is at  $\epsilon_c = -4.8$  eV and  $\Delta = 0$  corresponds to a  $M-M-M$  junction; see Fig. 1(a)], exploring the two cases of weakly coupled molecule (solid blue line) and strongly coupled molecule (dashed red line), as described above. For the weakly coupled molecule, we see an increase of a factor 2 from the  $M-M-M$  junction to the optimal band gap. For the strongly coupled junction, we find that  $ZT$  can rise as high as approximately 0.6, with a 4-orders-of-magnitude increase in  $ZT$  compared to the  $M-M-M$  junctions. The inset shows  $S$  as a function of  $\Delta$  and both the weakly coupled and strongly coupled molecules exhibit orders-of-magnitude increase in  $S$  compared to the  $M-M-M$  junctions.

Finally, in Fig. 6, the temperature dependence of  $ZT$  is examined for the weakly coupled hybrid molecular junction evaluated for  $\epsilon_0 = -5.2$  eV [corresponding to the maximum in  $ZT$  from Fig. 4(d)] [the rest of the parameters are the same as in Figs. 4(a)–4(d)].  $ZT$  increases with temperature, exhibiting a maximum of  $ZT$  of approximately 0.9 at

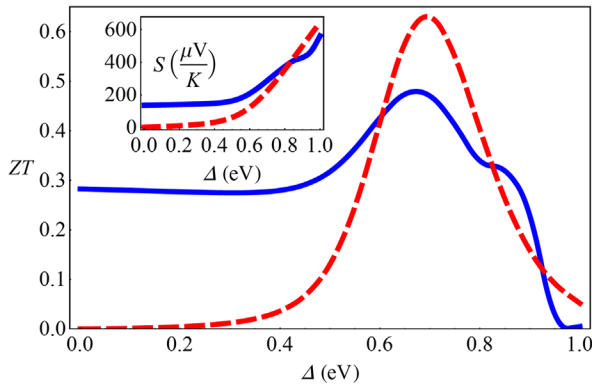


FIG. 5.  $ZT$  as a function of the SC-NP band gap  $\Delta$  at constant molecular level  $\epsilon_0 = -5.2$  eV, for weakly coupled (solid blue line) and strongly coupled (dashed red line) molecule. Inset:  $S$  as a function of  $\Delta$ .

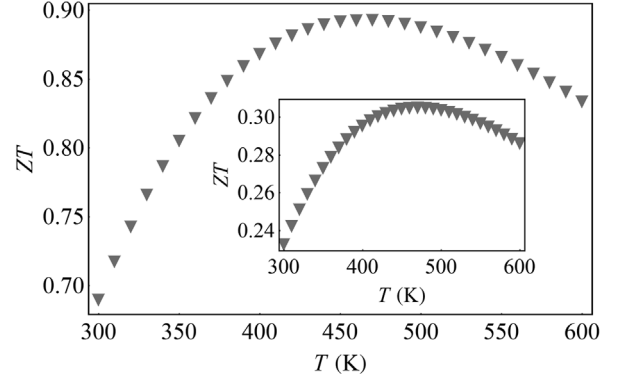


FIG. 6. Temperature dependence of  $ZT$  for  $\epsilon_0 = -5.16$  eV. Inset: Same but with  $\kappa_{\text{ph}} = 150$  pW/K.

$T \sim 450$  K, followed by a moderate decrease. This finding again implies that relatively large values of  $ZT$  persist in a broad range of parameters. In fact, in the inset of Fig. 5, we plot  $ZT$  calculated with an overevaluated value of the phonon thermal conductance  $\kappa_{\text{ph}} = 150$  pW/K, and we find that  $ZT$  reaches values of approximately 0.3, which is still several orders of magnitude larger than the observed values.

#### IV. SUMMARY AND CONCLUSIONS

In summary, we present calculations of thermopower and thermoelectric FOM for a hybrid metal–single-molecule–semiconducting-nanoparticle–metal molecular junction. The presence of the SC NP and the position of the molecular orbital close to the semiconducting band edge enhance the particle-hole asymmetry required for efficient thermoelectric conversion. The resulting values of thermopower and  $ZT$  are much larger than those measured in experiments and reach values as high as  $S \sim 500$   $\mu\text{V}/\text{K}$  and  $ZT$  of approximately 1 (an improvement of 4 orders of magnitude over measured molecular junctions). We show that this enhanced thermoelectric performance persists over a wide range of parameters and is robust against disorder in the form of surface-attached molecules. We show that decoherence at the molecule-nanoparticle boundary is not detrimental to the thermoelectric performance and that large values of  $ZT$  persist up to high temperatures. Comparing hybrid SC-NP–molecule junctions to the more “standard” metal-molecule-metal junction, we find that for weakly coupled molecules there is a factor of approximately 2 increase in  $ZT$  and a factor approximately 4 in the thermopower. For strongly coupled molecules, the advantage of hybrid NP-molecule junctions is even more profound, with (2–4)-orders-of-magnitude increase in  $ZT$  and thermopower in hybrid junctions.

The model we present here is a generic model, not aimed at any specific system. Nevertheless, our numerical parameters are taken from an experimentally observed value, including the phononic contribution to the thermal conductance. This, along with the fact that enhanced thermoelectric performance

is found for a wide range of molecular parameters and is robust against disorder, decoherence, and high temperatures, strongly suggest that high values of thermopower can be reached in future experiments on molecule-nanoparticle junctions, which are promising candidates for nanoscale thermoelectric conversion.

### ACKNOWLEDGMENTS

The authors acknowledge funding from the BGU-UM joint research initiative (Adelis Foundation).

- 
- [1] Arieh Aviram and Mark A. Ratner, Molecular rectifiers, *Chem. Phys. Lett.* **29**, 277 (1974).
- [2] Sriharsha V. Aradhya and Latha Venkataraman, Single-molecule junctions beyond electronic transport, *Nat. Nanotechnol.* **8**, 399 (2013).
- [3] Makusu Tsutsui and Masateru Taniguchi, Single molecule electronics and devices, *Sensors* **12**, 7259 (2012).
- [4] Y. Dubi and M. Di Ventra, Colloquium: Heat flow and thermoelectricity in atomic and molecular junctions, *Rev. Mod. Phys.* **83**, 131 (2011).
- [5] Lon E. Bell, Cooling, heating, generating power, and recovering waste heat with thermoelectric systems, *Science* **321**, 1457 (2008).
- [6] *Nanoscale Thermoelectrics*, edited by Xiaodong Wang and Zhiming M. Wang (Springer, New York, 2014).
- [7] G. D. Mahan and J. O. Sofo, The best thermoelectric, *Proc. Natl. Acad. Sci. U.S.A.* **93**, 7436 (1996).
- [8] Pdraig Murphy, Subroto Mukerjee, and Joel Moore, Optimal thermoelectric figure of merit of a molecular junction, *Phys. Rev. B* **78**, 161406 (2008).
- [9] J. P. Bergfield and C. A. Stafford, Thermoelectric signatures of coherent transport in single-molecule heterojunctions, *Nano Lett.* **9**, 3072 (2009).
- [10] Justin P. Bergfield, Michelle A. Solis, and Charles A. Stafford, Giant thermoelectric effect from transmission supernodes, *ACS Nano* **4**, 5314 (2010).
- [11] C. M. Finch, V. M. Garcia-Suarez, and C. J. Lambert, Giant thermopower and figure of merit in single-molecule devices, *Phys. Rev. B* **79**, 033405 (2009).
- [12] O. Karlström, H. Linke, G. Karlström, and A. Wacker, Increasing thermoelectric performance using coherent transport, *Phys. Rev. B* **84**, 113415 (2011).
- [13] D. Nozaki, H. Sevinçli, W. Li, R. Gutiérrez, and G. Cuniberti, Engineering the figure of merit and thermopower in single-molecule devices connected to semiconducting electrodes, *Phys. Rev. B* **81**, 235406 (2010).
- [14] Robert Stadler and Troels Markussen, Controlling the transmission line shape of molecular *t*-stubs and potential thermoelectric applications, *J. Chem. Phys.* **135**, 154109 (2011).
- [15] Hisao Nakamura, Tatsuhiko Ohto, Takao Ishida, and Yoshihiro Asai, Thermoelectric efficiency of organometallic complex wires via quantum resonance effect and long-range electric transport property, *J. Am. Chem. Soc.* **135**, 16545 (2013).
- [16] Jaroslav Vacek, Jana Vacek Chocholousova, Irena G. Stara, Ivo Stary, and Yonatan Dubi, Mechanical tuning of conductance and thermopower in helicene molecular junctions, *Nanoscale* **7**, 8793 (2015).
- [17] J. A. Malen, P. Doak, K. Baheti, T. D. Tilley, A. Majumdar, and R. A. Segalman, The nature of transport variations in molecular heterojunction electronics, *Nano Lett.* **9**, 3406 (2009).
- [18] J. A. Malen, P. Doak, K. Baheti, T. D. Tilley, R. A. Segalman, and A. Majumdar, Identifying the length dependence of orbital alignment and contact coupling in molecular heterojunctions, *Nano Lett.* **9**, 1164 (2009).
- [19] J. A. Malen, S. K. Yee, A. Majumdar, and R. A. Segalman, Fundamentals of energy transport, energy conversion, and thermal properties in organic-inorganic heterojunctions, *Chem. Phys. Lett.* **491**, 109 (2010).
- [20] P. Reddy, S. Y. Jang, R. A. Segalman, and A. Majumdar, Thermoelectricity in molecular junctions, *Science* **315**, 1568 (2007).
- [21] Jonathan R. Widawsky, Pierre Darancet, Jeffrey B. Neaton, and Latha Venkataraman, Simultaneous determination of conductance and thermopower of single molecule junctions, *Nano Lett.* **12**, 354 (2012).
- [22] Jonathan R. Widawsky, Wenbo Chen, Hector Vazquez, Taekyeong Kim, Ronald Breslow, Mark S. Hybertsen, and Latha Venkataraman, Length-dependent thermopower of highly conducting Au-C bonded single molecule junctions, *Nano Lett.* **13**, 2889 (2013).
- [23] William B. Chang, Cheng-Kang Mai, Michele Kotiuga, Jeffrey B. Neaton, Guillermo C. Bazan, and Rachel A. Segalman, Controlling the thermoelectric properties of thiophene-derived single-molecule junctions, *Chem. Mater.* **26**, 7229 (2014).
- [24] Youngsang Kim, Wonho Jeong, Kyeongtae Kim, Wochul Lee, and Pramod Reddy, Electrostatic control of thermoelectricity in molecular junctions, *Nat. Nanotechnol.* **9**, 881 (2014).
- [25] Janakiraman Balachandran, Pramod Reddy, Barry D. Dunietz, and Vikram Gavini, End-group-induced charge transfer in molecular junctions: Effect on electronic structure and thermopower, *J. Phys. Chem. Lett.* **3**, 1962 (2012).
- [26] See Kei Lee, Tatsuhiko Ohto, Ryo Yamada, and Hirokazu Tada, Thermopower of benzenedithiol and C60 molecular junctions with Ni and Au electrodes, *Nano Lett.* **14**, 5276 (2014).
- [27] M. Di Ventra, *Electrical Transport in Nanoscale Systems* (Cambridge University Press, Cambridge, England, 2008).
- [28] Elke Scheer and Juan Carlos Cuevas, *Molecular Electronics: An Introduction to Theory and Experiment* (World Scientific, Singapore, 2010), Vol. 1.
- [29] Christophe Goupil, Wolfgang Seifert, Knud Zabrocki, Eckhart Müller, and G. Jeffrey Snyder, Thermodynamics of thermoelectric phenomena and applications, *Entropy* **13**, 1481 (2011).
- [30] Cronin B. Vining, An inconvenient truth about thermoelectrics, *Nat. Mater.* **8**, 83 (2009).
- [31] Wee-Liat Ong, Shubhaditya Majumdar, Jonathan A. Malen, and Alan J. H. McGaughey, Coupling of organic and

- inorganic vibrational states and their thermal transport in nanocrystal arrays, *J. Phys. Chem. C* **118**, 7288 (2014).
- [32] Dvira Segal, Abraham Nitzan, and Peter Hänggi, Thermal conductance through molecular wires, *J. Chem. Phys.* **119**, 6840 (2003).
- [33] Zhaohui Wang, Jeffrey A. Carter, Alexei Lagutchev, Yee Kan Koh, Nak-Hyun Seong, David G. Cahill, and Dana D. Dlott, Ultrafast flash thermal conductance of molecular chains, *Science* **317**, 787 (2007).
- [34] Stefan Ballmann and Heiko B. Weber, An electrostatic gate for mechanically controlled single-molecule junctions, *New J. Phys.* **14**, 123028 (2012).
- [35] Brian Capozzi, Qishui Chen, Pierre Darancet, Michele Kotiuga, Marisa Buzzeo, Jeffrey B. Neaton, Colin Nuckolls, and Latha Venkataraman, Tunable charge transport in single-molecule junctions via electrolytic gating, *Nano Lett.* **14**, 1400 (2014).
- [36] Ferry Prins, Amelia Barreiro, Justus W. Ruitenbergh, Johannes S. Seldenthuis, Nria Aliaga-Alcalde, Lieven M. K. Vandersypen, and Herre S. J. van der Zant, Room-temperature gating of molecular junctions using few-layer graphene nanogap electrodes, *Nano Lett.* **11**, 4607 (2011).
- [37] Victor I. Klimov, *Semiconductor and Metal Nanocrystals: Synthesis and Electronic and Optical Properties* (CRC Press, New York, NY, 2003).
- [38] Uri Banin and Oded Millo, Tunneling and optical spectroscopy of semiconductor nanocrystals, *Annu. Rev. Phys. Chem.* **54**, 465 (2003).
- [39] Dmitri V. Talapin, Jong-Soo Lee, Maksym V. Kovalenko, and Elena V. Shevchenko, Prospects of colloidal nanocrystals for electronic and optoelectronic applications, *Chem. Rev.* **110**, 389 (2010).
- [40] Jianhui Liao, Laetitia Bernard, Michael Langer, Christian Schönenberger, and Michel Calame, Reversible formation of molecular junctions in 2d nanoparticle arrays, *Adv. Mater.* **18**, 2444 (2006).
- [41] S. Hassan M. Jafri, Tobias Blom, Klaus Leifer, Maria Strömme, Henrik Löfström, Anton Grigoriev, Rajeev Ahuja, and Ken Welch, Assessment of a nanoparticle bridge platform for molecular electronics measurements, *Nanotechnology* **21**, 435204 (2010).
- [42] Wei Huang, Gou Masuda, Seisuke Maeda, Hirofumi Tanaka, and Takuji Ogawa, Molecular junctions composed of oligothiophene dithiol-bridged gold nanoparticles exhibiting photoresponsive properties, *Chemistry* **12**, 607 (2006).
- [43] Boris Fainberg and Tamar Seideman, Photoinduced current in molecular conduction junctions with semiconductor contacts, *Phys. Status Solidi (a)* **209**, 2433 (2012).
- [44] Matthew G. Reuter, Thorsten Hansen, Tamar Seideman, and Mark A. Ratner, Molecular transport junctions with semiconductor electrodes: Analytical forms for one-dimensional self-energies?, *J. Phys. Chem. A* **113**, 4665 (2009).
- [45] Christophe Delerue and Michel Lannoo, *Nanostructures: Theory and Modelling* (Springer Science & Business Media, New York, 2004).
- [46] Günter Schmid, *Nanoparticles: From Theory to Application* (John Wiley & Sons, New York, 2011).
- [47] J. G. Diaz, J. Planelles, G. W. Bryant, and J. Aizpurua, Tight-binding method and multiband effective mass theory applied to CdS nanocrystals: Single-particle effects and optical spectra fine structure, *J. Phys. Chem. B* **108**, 17800 (2004).
- [48] Nicola A. Hill and K. Birgitta Whaley, A theoretical study of the influence of the surface on the electronic structure of CdSe nanoclusters, *J. Chem. Phys.* **100**, 2831 (1994).
- [49] Tianshu Li and Giulia Galli, Electronic properties of MoS<sub>2</sub> nanoparticles, *J. Phys. Chem. C* **111**, 16192 (2007).
- [50] Jon M. Azpiroz, Jesus M. Ugalde, and Ivan Infante, Benchmark assessment of density functional methods on group II-VI MX ( $M = \text{Zn, Cd}$ ;  $X = \text{S, Se, Te}$ ) quantum dots, *J. Chem. Theory Comput.* **10**, 76 (2014).
- [51] Yigal Meir, Ned S. Wingreen, and Patrick A. Lee, Transport through a Strongly Interacting Electron System: Theory of Periodic Conductance Oscillations, *Phys. Rev. Lett.* **66**, 3048 (1991).
- [52] F. M. Souza, J. C. Egues, and A. P. Jauho, Quantum dot as a spin-current diode: A master-equation approach, *Phys. Rev. B* **75**, 165303 (2007).
- [53] Yigal Meir and Ned S. Wingreen, Landauer Formula for the Current through an Interacting Electron Region, *Phys. Rev. Lett.* **68**, 2512 (1992).
- [54] C. J. O. Verzijl, J. S. Seldenthuis, and J. M. Thijssen, Applicability of the wide-band limit in DFT-based molecular transport calculations, *J. Chem. Phys.* **138**, 094102 (2013).
- [55] S. Datta, *Electronic Transport in Mesoscopic Systems* (Cambridge University Press, Cambridge, England, 1997).
- [56] Uri Peskin, An introduction to the formulation of steady-state transport through molecular junctions, *J. Phys. B* **43**, 153001 (2010).
- [57] P. K. Khanna, Ki-Won Jun, Anisha Gokarna, Jin-Ook Baeg, and Sang Il Seok, One-step synthesis of {TOP} capped PbSe pyramidal nanocrystals, *Mater. Chem. Phys.* **96**, 154 (2006).
- [58] Chang-Wei Wang, Hong-Guo Liu, Xiang-Tao Bai, Qingbin Xue, Xiao Chen, Yong-Ill Lee, Jingcheng Hao, and Jianzhuang Jiang, Triangular PbS nano-pyramids, square nanoplates, and nanorods formed at the air/water interface, *Cryst. Growth Des.* **8**, 2660 (2008).
- [59] Magnus Paulsson and Supriyo Datta, Thermoelectric effect in molecular electronics, *Phys. Rev. B* **67**, 241403 (2003).
- [60] Jianfeng Zhou, Satyabrata Samanta, Cunlan Guo, Jason Locklin, and Bingqian Xu, Measurements of contact specific low-bias negative differential resistance of single metalorganic molecular junctions, *Nanoscale* **5**, 5715 (2013).
- [61] Jianfeng Zhou, Guojun Chen, and Bingqian Xu, Probing the molecule- electrode interface of single-molecule junctions by controllable mechanical modulations, *J. Phys. Chem. C* **114**, 8587 (2010).
- [62] Ismael Diez-Perez, Joshua Hihath, Thomas Hines, Zhong-Sheng Wang, Gang Zhou, Klaus Müllen, and Non-gjian Tao, Controlling single-molecule conductance through lateral coupling of  $\pi$  orbitals, *Nat. Nanotechnol.* **6**, 226 (2011).
- [63] Jie Ren, Jian-Xin Zhu, James E. Gubernatis, Chen Wang, and Baowen Li, Thermoelectric transport with electron-phonon coupling and electron-electron interaction in molecular junctions, *Phys. Rev. B* **85**, 155443 (2012).
- [64] Gerald D. Mahan, *Many-Particle Physics* (Springer, New York, 2000).